Equatorial Atmospheric and Ionospheric Modeling at Kwajalein Missile Range

Stephen M. Hunt, Sigrid Close, Anthea J. Coster, Eric Stevens, Linda M. Schuett, and Anthony Vardaro

During the last peak of the solar activity cycle, in the late 1980s and early 1990s, the spatial and temporal variations of the equatorial ionosphere had a significant impact on the measurement accuracy of the ARPA Long-Range Tracking and Instrumentation Radar (ALTAIR) at the Kwajalein Missile Range (KMR), primarily because of poorly modeled ionospheric range and elevation-angle bias errors. As missile-reentry-vehicle and space-surveillance missions have developed at KMR, improvements in ALTAIR measurement accuracy have illustrated that unmodeled atmospheric refraction is the principal error source limiting sensor accuracy. Modeling equatorial ionospheric activity and then removing its effect on KMR data is particularly challenging, since the radar is located beneath a complex region of the earth's ionosphere. To characterize the spatial and temporal electron distribution in the ionosphere, real-time measurement data are required to adjust the models to match actual conditions. An effort to better characterize both peak and disturbed ionospheric conditions in real time has resulted in the ionospheric error-correction model (IECM). This article discusses the KMR atmospheric models, and presents representative equatorial ionospheric data as viewed by ALTAIR along with an evaluation of the IECM at removing these range and elevation-angle bias errors.

To track satellites and ballistic-missile reentry vehicles, high-power radar systems at the Kwajalein Missile Range (KMR) transmit signals at frequencies spanning 160 MHz to 95 GHz. Frequency-dependent signal-propagation effects produced in the atmosphere can degrade the accuracy of measurements collected by these radar systems. Since these radars collect position, velocity, and radar cross-section data on objects that traverse the troposphere (the lower atmosphere) and the ionosphere (above ninety kilometers), we have spent many years developing spatial-dependent and time-dependent radio-frequency (RF) signal-propagation models that mitigate atmospheric signal degradation. These models consist of two main components: (1) the spatial-varying and time-varying nature of the index of refraction in each region of the atmosphere, and (2) the corresponding RF signal-propagation effects themselves.

Kwajalein Atoll is located in the Marshall Islands in the Pacific Ocean, approximately four thousand kilometers southwest of Hawaii. It consists of approximately one hundred small islands resting on a coral reef formation eleven hundred kilometers north of the geographic equator. The two principal islands are Kwajalein and Roi-Namur. The KMR radars are located on Roi-Namur, where they support ballistic-missile-test and space-surveillance missions. The radars at KMR collect highly accurate metric and radar cross-section data to characterize missile-reentry vehicles as well as help maintain the U.S. Space Command catalog of artificial satellites. The primary radar for this latter task is the Advanced Research Projects Agency (ARPA) Long-Range Tracking and Instrumentation Radar, or ALTAIR, which is a two-frequency (160 and 422 MHz) radar located on Roi-Namur at 4° north geomagnetic latitude.

A notable and significant difference between missile-reentry-vehicle data processing and space-surveillance data processing is that reentry-vehicle data are post-processed to obtain maximum metric accuracy, while space-surveillance data must be accurately corrected in real time and immediately transmitted to U.S. Space Command. ALTAIR performs most of the satellite tracking for U.S. Space Command at KMR, and it is dedicated to this task 128 hours per week.

This article provides an overview of the KMR equatorial atmospheric environment, the first-order ALTAIR atmospheric-correction model, and the new ionospheric error-correction model (IECM). The article also presents radar calibration data to illustrate the accuracy obtained while correcting metric observations with the IECM and the first-order ALTAIR model. We also present an overview of two-frequency total electron content (TEC) data reduction and its application, along with a section describing what we learned during years of experimentation with Global Positioning System (GPS) receivers for the purpose of real-time TEC data collection.

Phenomenology of the Equatorial Ionosphere

As the altitude above the earth increases, the density of the atmosphere decreases. The first ninety kilometers of the atmosphere are basically neutral and consist of a homogeneous mixture of several gases with three primary layers: the troposphere (approximately zero to fifteen kilometers in altitude), the stratosphere (fifteen to fifty kilometers in altitude), and the mesosphere (fifty to ninety kilometers in altitude) [1]. These atmospheric layers are generally distinct; they are well mixed by turbulence, which is primarily the result of thermal winds coupled with forces from the earth's rotation. During the daytime, weak ionization begins to develop in the mesosphere, which serves as a transition region to the ionosphere.

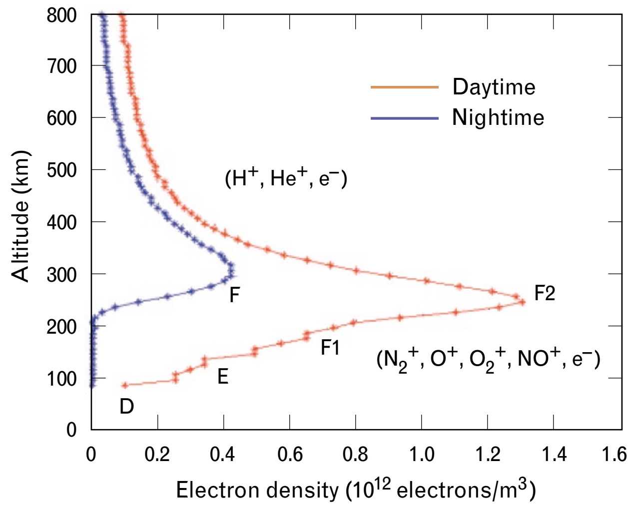

FIGURE 1. Typical altitude profile of ionospheric electron density. Free electrons, molecular ions, and atomic ions form into distinct layers during the daytime—the D, E, F1, and F2 regions—while the F1 and F2 regions combine during the diminished solar activity of the evening hours to form the F region. Heavier atoms and molecules (N_2, O, O_2) tend to reside near the bottom of the ionosphere, while lighter atoms and molecules (H, He) are found near the top. The net charge of the plasma found in the ionosphere is generally neutral. The Kwajalein Missile Range (KMR) atmospheric correction models take into account the radio-frequency (RF) propagation effects caused by the presence of free electrons.

Above an altitude of approximately ninety kilometers the gases are strongly ionized by solar radiation, as shown in Figure 1. At this higher altitude, which is the region known as the ionosphere, the ionized gases no longer tend to be uniformly mixed; heavy gas molecules and atoms such as nitrogen and oxygen are found near the bottom of the ionosphere, and lighter gas molecules and atoms such as hydrogen and helium are found near the top. Free electrons and ions (both molecular and atomic) are present in nearly equal numbers in this region, which results in an overall (net) neutral charge for the particle distribution. The distribution and dynamics of these particles in the ionosphere affect the propagation of radio waves and the corresponding radar measurements of objects within or above the ionosphere.

A plasma is defined as a collection of positively charged atoms and molecules with negatively charged electrons in approximately equal numbers, with an overall net charge of zero. Because the earth has a strong magnetic field relative to any induced magnetic fields resulting from the motion of charged particles in the ionospheric plasma, the plasma distribution resulting from the dynamical aspects of the ionosphere is normally dominated by the earth's dipole magnetic field. At the equator and above the ionosphere, an enhanced electron density region exists (called the plasmasphere) that can extend to several earth radii. There is no static boundary between the ionosphere and the plasmasphere; for this article we define the region above two thousand kilometers to be the plasmasphere.

During the daytime, several distinct layers are formed in the upper atmosphere, including the D region within the mesosphere (50 to 90 km altitude), and the E region (90 to 120 km altitude) and the F1 and F2 regions (120 to 600+ km altitude) within the ionosphere. At nighttime the D and E regions become neutral and the F1 and F2 layers often merge into a single F region, characterized by reduced electron density, as shown in Figure 1. Distinct ionospheric regions develop for three primary reasons: (1) the solar spectrum deposits its energy at various heights, depending on the absorption characteristics of the atmosphere, (2) the physics of recombination depends on density, and (3) the composition of the atmosphere changes with height [2].

The location of the peak electron density and the shape of the ionospheric layers depend greatly on a number of factors and are therefore highly variable. A standard ionospheric profile can be generated by Chapman theory, which provides a closed-form analytic description of ion (and corresponding electron) production in the upper atmosphere, and results in a quasi-exponential distribution of free electrons with altitude. The terms "ionospheric anomaly" and "ionospheric irregularity" are used to describe conditions that are not described by the Chapman ionization function [3]. (Even in its quiet state, with no anomalies or irregularities, the ionosphere is often not described by a simple Chapman function, which is why more sophisticated models are generally required.) An ionospheric anomaly can be thought of as a medium-to-large-scale disturbance in the background ionosphere, such as the mid-latitude trough regions associated with magnetic storms. Ionospheric irregularities are typically small-to-medium-scale density fluctuations in the background ionosphere that are routinely present in the ionosphere, such as gravity waves or small-scale irregularities associated with scintillation.

Figure 2 shows GPS TEC data to illustrate the diurnal variation of the ionosphere. Rapid fluctuations in TEC during the early evening hours indicate the presence of ionospheric irregularities, which are more prevalent during increased solar activity. Figure 3 illustrates periodic changes in ionospheric activity that include seasonal and solar-cycle variations, all of which can be thought of as predictable. Figure 3 also shows the corresponding VHF range delay, which can be as great as 1700 m at ALTAIR's vertical (above 50°). When ALTAIR views satellites at the horizon, this VHF range delay is approximately three times greater (approximately 5100 m) because of the increased amount of atmosphere present along the radar line of sight.

The equatorial region is dominated by the anomalies and irregularities mentioned previously and outlined in Table 1. The equatorial ionosphere is strongly

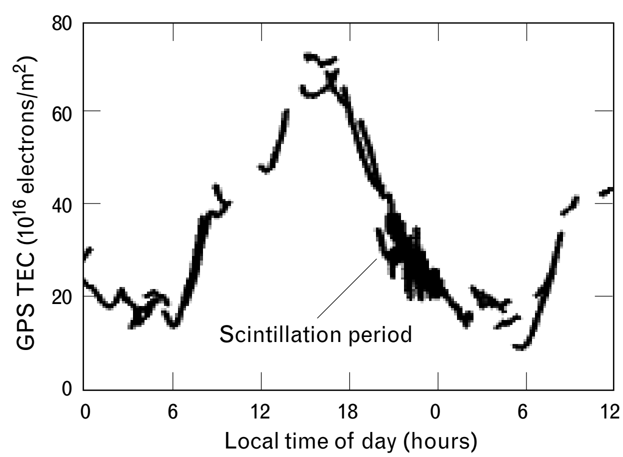

FIGURE 2. Illustration of the diurnal variation of the ionosphere, using Global Positioning System (GPS) total electron content (TEC) data collected during a thirty-six-hour period at ALTAIR's vertical (above 50° elevation). The rapid fluctuations in TEC shown during the scintillation period in the early evening hours illustrate the presence of ionospheric irregularities, which are more prevalent during increased solar activity. The increasing and decreasing trends even at high elevation angle indicate the complex ion distribution at ALTAIR's vertical.

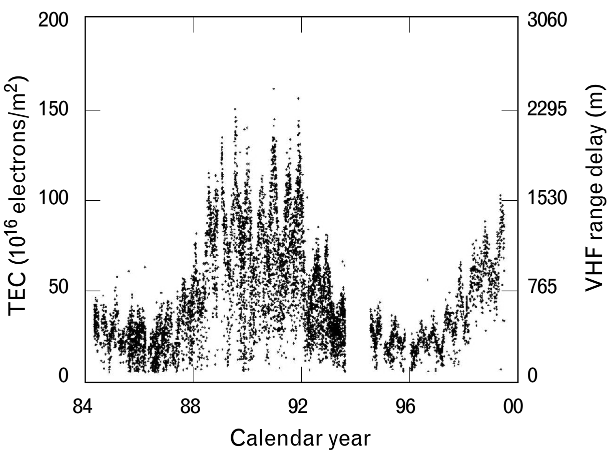

FIGURE 3. The eleven-year solar cycle as viewed from the geomagnetic equator. These data are two-frequency TEC measurements collected at ALTAIR since 1983. They are used to make a daily adjustment to the first-order ALTAIR ionospheric-correction model. One TEC unit is equivalent to 15.3 meters of range delay at VHF. Therefore, the magnitude of the ionospheric range delay reached approximately 1500 meters during the last peak in the solar activity cycle.

affected by the north-south orientation of magnetic-field lines lying parallel to the surface of the earth at the equator. At the equator, a strong eastward ionospheric current flows by day over a narrow latitudinal strip (a few degrees of latitude wide) along the magnetic equator at an altitude near 100 km. This current is known as the equatorial electrojet. Also present is the occurrence of the Appleton, or equatorial, anomaly. This anomaly is the electron-density depletion region that exists at the geomagnetic equator along with regions of enhanced electron density that peak at approximately 15° to 20° north and south latitude, as shown in Figure 4. This distribution is caused by the vertical electrodynamic drift of the equatorial plasma and its later diffusion along the north-south geomagnetic field lines (**B**). An east-west–oriented electric field (**E**) at the geomagnetic equator perpendicular to the north-south magnetic field causes this vertical $\mathbf{E} \times \mathbf{B}$ drift. The most disturbed scintillation region was observed at one of the crests of the Appleton anomaly during a sunspot maximum period [4].

Also observed on the equator are F-region irregularities caused by the existence of gravitational Rayleigh-Taylor instabilities (GRTs). GRTs result from an interaction between the downward gradient of the earth's gravitational field and the parallel orientation of the earth's equatorial electric and magnetic fields with the surface of the earth. A detailed treatment on the formation of this irregularity, which is beyond the scope of this article, is an area of ongoing research in equatorial aeronomy and plasma physics. Data on

Table 1. Irregularities and Anomalies Prevalent at Equatorial Locations

Type of variation	*Ionosphere region*	*Distribution*	*Time most prevalent*	*Duration*
Electrojet irregularities	E region	East-west	All times (stronger in daytime)	<30 minutes to hours
Appleton anomaly	Above the F region	Enhancement at 10–20° north-south (depletion at equator)	Late afternoon and early evening	>4 hours
Rayleigh-Taylor instabilities	F region	Along magnetic field lines (north-south)	After sunset and early evening	>2.5 hours
Magnetic-storm effects	E region and F region	Global	All times	Seconds to hours

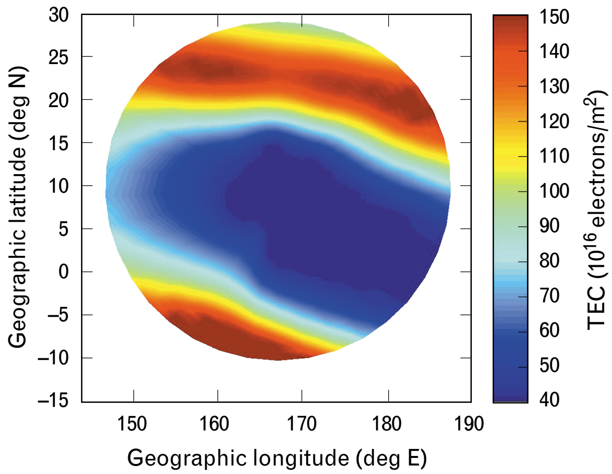

FIGURE 4. TEC map from the ionospheric error-correction model (IECM), illustrating the characteristic distribution of the Appleton anomaly. The dark red portions near 20° latitude are high electron-density regions. The blue section is the electron-depletion formation at the equator caused by the upward (**E** × **B**) and later north-south drift of electrons along the earth's magnetic field lines. The Appleton anomaly forms at the geomagnetic equator in the late afternoon and persists into the evening hours.

these irregularities were collected at the Jicamarca incoherent scatter radar in Peru at 12° south latitude [5]. Similar studies have been periodically conducted at ALTAIR since 1978 [6–9]. A continuous long-term study at Kwajalein would provide a significant contribution to the understanding of equatorial ionospheric irregularity phenomena. The outcome of this scientific research would apply directly to the development of techniques to mitigate the effects of these phenomena on RF signal propagation as applied to radar measurements and communications.

Large electron-density depletion regions persist in the F region during the early evening to early morning hours, and have complex scattering characteristics that are a source of intense RF scintillation and frequency-spreading (spread-F) conditions. RF scintillation describes the rapid fluctuation of amplitude and phase, while spread-F describes the signal frequency dispersion experienced by high-frequency ionospheric sounders during disturbed ionospheric conditions. Spread-F is a general term used to denote the existence of an ionospheric irregularity in RF measurement data. This term originated from data collected with vertical ionospheric sounders, which transmit across a broad high-frequency spectrum, because the resulting frequency signatures are spread in range relative to periods where irregularities are nonexistent [10]. As an example, Figure 5 shows 49.92-MHz coherent backscatter data collected by the Jicamarca radar facility in Peru at 12° south latitude and

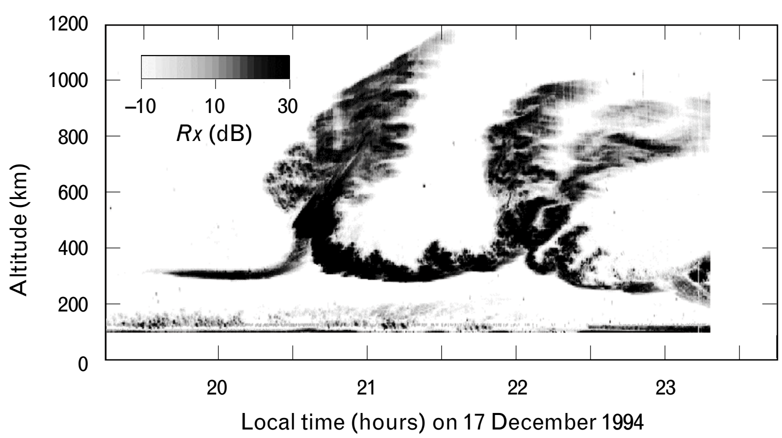

FIGURE 5. Range-time-intensity plot of received power (*Rx*) from the Jicamarca radar facility in Peru at 12° south latitude [11]. The Jicamarca operating frequency was 49.92 MHz. These large structures are most likely due to electron-density depletion regions caused by gravitational Rayleigh-Taylor instabilities. Presumably, Jicamarca experiences ionospheric conditions similar to those at ALTAIR, given its close proximity to the equator. Most of ALTAIR's operating time is spent on space-surveillance and missile-reentry-vehicle tests, but its incoherent scatter radar capability is periodically used to support experimental research to better characterize the equatorial atmosphere. (Image courtesy of *Geophysical Research Letters* [11], copyright by the American Geophysical Union.)

285° east longitude, which show spread-F conditions caused by the presence of a large irregularity.

Figure 6 illustrates radar measurements collected by ALTAIR while it was tracking eight reentering objects, all on the same basic flight-path trajectory, as they traversed one of these equatorial irregularity regions. The trajectory and the variation in radar-return signal characteristics (RF scintillation) on these objects are consistent with the size and distribution of the irregularity shown in Figure 5. The latitude-longitude-height orientation of the ALTAIR measurements illustrates evidence of an irregularity region that extends to the north in latitude and to the west in longitude, and spanning at least a hundred kilometers in altitude.

Modeling the Atmosphere

Radar tracking of satellites is complicated by several effects introduced by the earth's atmosphere. Figure 7 illustrates how the atmosphere distorts RF measurements and causes the position of targets to appear offset relative to their true location. Apparent position refers to the measured range and elevation angle of the satellite in the presence of the atmosphere. The true position refers to the range and elevation angle of the satellite with atmospheric effects removed.

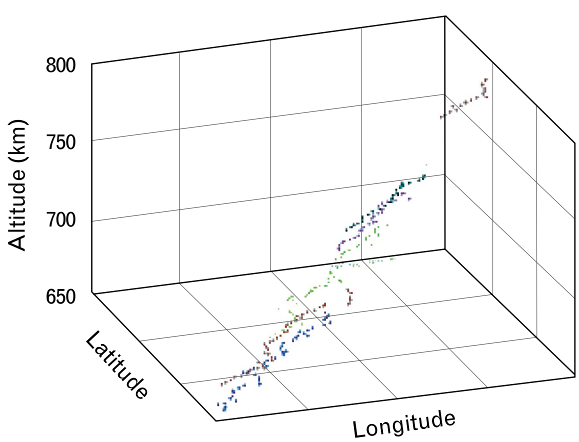

FIGURE 6. ALTAIR data collected while eight missile-reentry vehicles traversed an equatorial ionospheric irregularity. The data shown here were measured while the vehicles were inside the irregularity. The RF return signals exhibited rapid fluctuations in amplitude and phase. As the spatial distribution of the measurement data increases in altitude, it also extends to the north in latitude and west in longitude. This distribution is indicative of an equatorial electron-depletion region resulting from a gravitational Rayleigh-Taylor instability, such as shown in Figure 5.

During the 1960s and the early 1970s, an effort was initiated to model the effects of the changing atmosphere (space weather effects on the ionosphere and terrestrial weather on the neutral atmosphere) on KMR radar measurements. The goal was to improve the accuracy of the radar data. The models developed for both the ionosphere and the neutral atmosphere were designed to create a true estimate of target position by removing the atmospheric effects that produce a distorted apparent target position. RF propagation effects include elevation-angle bending, range delay, Doppler frequency shifts, polarization rotation, frequency spreading, and rapid amplitude and phase scintillation. The KMR atmospheric models are primarily focused on correcting for the effects that are responsible for radar-range (time delay) and elevation-angle bias errors.

The early atmospheric refraction models developed for KMR sensors were produced by D.W. Blood and D. Kwan. These models are used to remove the effects of the neutral atmosphere (below 90 km) on radar measurements. Later, ionospheric correction methods were added by T. Pass, using simultaneous two-frequency radar range measurements combined with an elevation-angle mapping function. As ALTAIR single-frequency tracking requirements expanded for space surveillance, a first-order vertical ionospheric range-delay model was added by R. McSheehy [12]. This first-order model maintains a continuous knowledge of ALTAIR's vertical ionospheric range delay, which enabled the operation of the radar for extended periods of time without the need to track at two frequencies to perform ionospheric correction.

In 1989, a measurement-accuracy shortfall was experienced at ALTAIR during the last peak of the solar activity cycle because of the limitations of the first-order single-frequency ionospheric model. This accuracy problem motivated the effort to replace the first-order ionospheric model with the IECM, which was developed for ALTAIR under a small-business innovative research contract by Research Associates of Syracuse, Inc., Syracuse, New York, and Computational Physics, Inc., Newton, Massachusetts [14, 15].

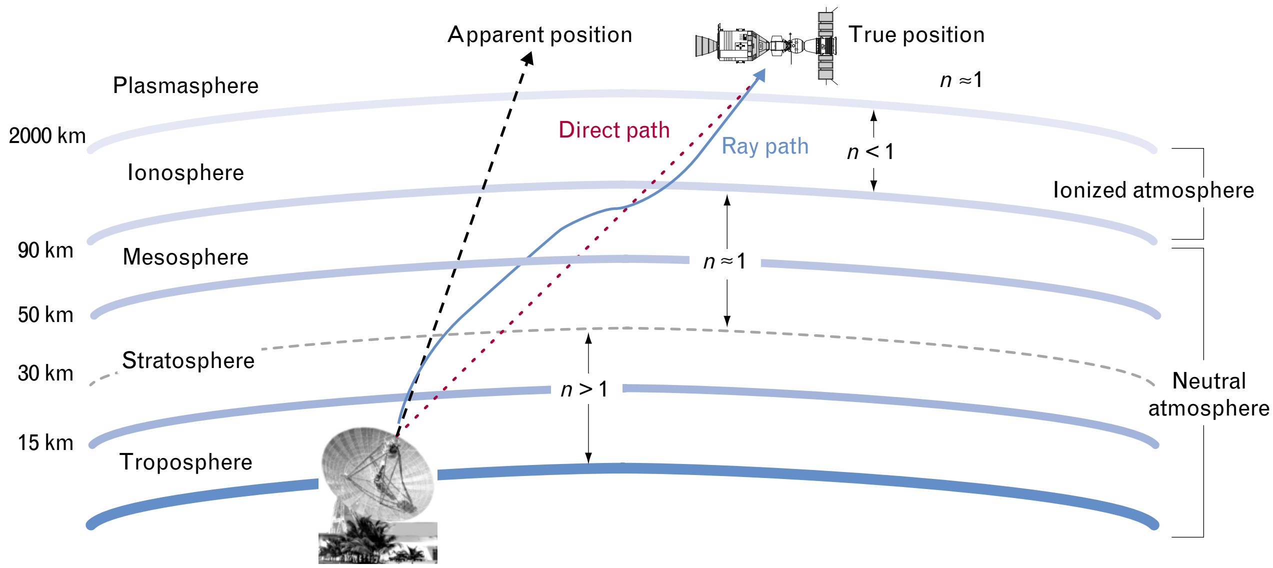

FIGURE 7. Illustration of the two-dimensional ray-traced path of a transmitted RF signal from the earth's surface through the neutral and ionized atmosphere. The ray-tracing algorithm uses range and elevation-angle corrections derived from the altitude-dependent index of refraction *n* to accurately determine satellite position.

The focus of the IECM development effort was to increase the accuracy of the real-time space-surveillance measurement data by providing an improved ionospheric modeling capability. The IECM combines a climatological low-latitude ionospheric model driven by real-time Global Positioning System (GPS) and ALTAIR total electron content (TEC) measurements. The early atmospheric-correction model developed by Blood and Kwan is used in the IECM to remove neutral atmospheric effects. The physics and chemistry of the upper atmosphere are based on the low-latitude ionospheric model developed by D.N. Anderson et al. in 1987 [16] and a plasmaspheric model developed by D.L. Gallagher [17]. Figure 8 illustrates the process of using the IECM to accurately measure satellite range and elevation angle. The enhanced capability of the IECM resulted in a significant improvement in the range accuracy of metric data collected during ALTAIR's continuous high-volume satellite-tracking operation. The IECM has been operational at ALTAIR since the spring of 1998.

The Index of Refraction in the Neutral and Ionized Atmosphere

To support the collection of accurate RF measurements (azimuth, elevation angle, range, and range rate) made by KMR radars, we require knowledge of the real-time atmospheric index of refraction as a function of altitude for the neutral atmosphere, ionosphere, and plasmasphere. The effects on radio signals in the neutral and ionized regions of the atmosphere are different. The ionosphere and plasmasphere are dispersive mediums with an index of refraction that is, to first order, a function of electron density and radio-wave frequency. The refraction effects are significantly larger at lower frequencies (as a result, the effect of the ionosphere at VHF is nearly a hundred times the effect at L-band). The index of refraction in the neutral atmosphere is a function of pressure, temperature, and humidity.

When RF signals propagate through the neutral atmosphere, they are subject to a spatial-varying and time-varying index of refraction that, to a first approximation, affects all KMR radars equally. The neutral atmosphere is thus a nondispersive medium at radio-wave frequencies. The KMR model of the index of refraction uses a mean refractivity profile to model the neutral atmosphere. This mean profile is based on radiosonde data collected at Kwajalein from 1967 to 1972. The model has a piecewise exponential form and is used to provide range and elevation-angle bias corrections. Some ionization exists in the upper

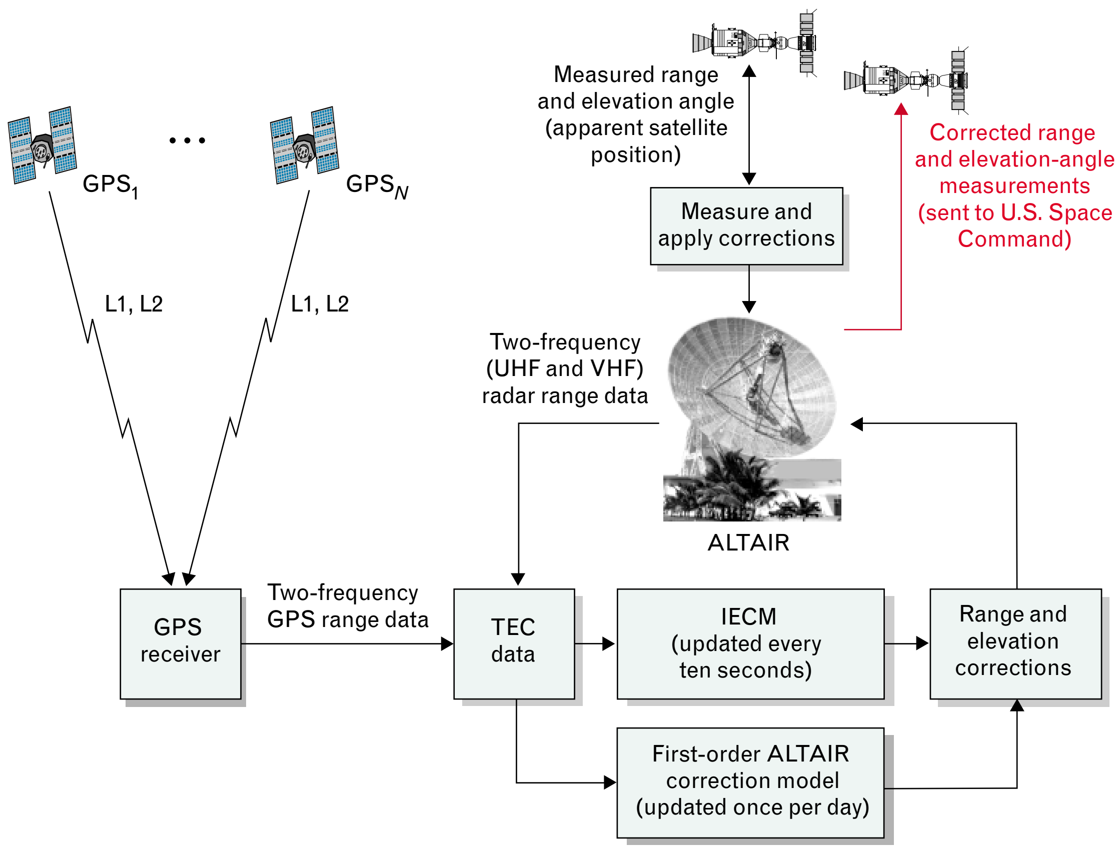

FIGURE 8. Ionospheric measurement and correction of space-surveillance range and elevation-angle data with the ARPA Long-Range Tracking and Instrumentation Radar (ALTAIR). Real-time two-frequency (L1 and L2) GPS range data, from a constellation of GPS satellites, and ALTAIR two-frequency (UHF and VHF) measured range data are used to support real-time ionospheric correction. These GPS and ALTAIR data are used by the new real-time ionospheric error-correction model (IECM) to compute range and elevation-angle corrections. Real-time corrections are supplied to the ALTAIR satellite-tracking software to remove ionosphere-induced range and elevation-angle errors from the ALTAIR measurements. Also shown is the old ALTAIR first-order atmospheric-correction model, which is adjusted by using a single ALTAIR measurement once per day.

Table 2. Blood and Kwan Exponential Refractivity Model

Profile region	*Altitude range (km)*	α *(N-units)*	β *(km^{-1})*
1	0.0 to 0.3048	378.0	0.21522
2	0.3048 to 0.6096	368.58	0.13255
3	0.6096 to 0.9144	375.57	0.16339
4	0.9144 to 4.1453	374.0	0.15879
5	4.1453 to 8.9916	329.0	0.12795
6	8.9916 to 15.0266	293.0	0.11549
7	above 15.0266	780.0	0.18045

stratosphere and lower mesosphere (from fifty to ninety kilometers in altitude), even though the KMR models define the dominating constituents as neutral. The ionospheric models do not come into effect until approximately ninety kilometers in altitude. The exponential refractivity N, which is related to the index of refraction n by the relation $N = (n - 1) \times 10^6$, is defined as

$$N = \alpha e^{-\beta h} , \qquad (1)$$

where α and β are altitude-dependent constants, and h is used to specify seven altitude regions. Table 2 lists the altitude ranges of the seven regions, and shows the associated values of the constants α and β in each of the regions.

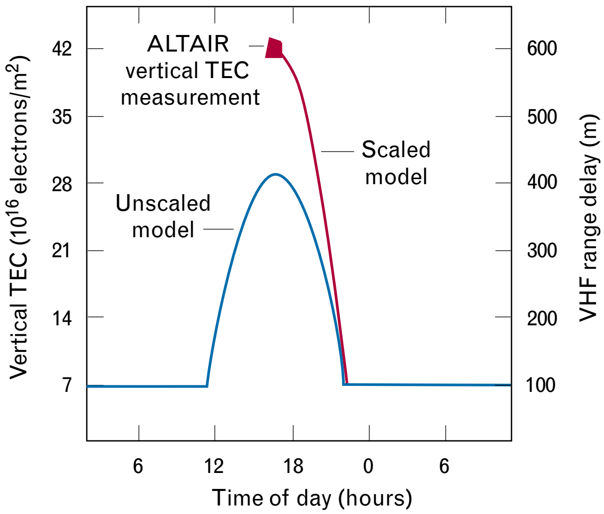

FIGURE 9. The ALTAIR first-order ionospheric range-delay model. This model, derived from ALTAIR ionospheric backscatter data and the first-order worldwide ionospheric Klobuchar model [13], is used to maintain continuous knowledge of the ionospheric range delay above ALTAIR. An unscaled analytic model provides a theoretical estimate of the vertical range delay at a given time of day. This model is then scaled by using a daily ALTAIR two-frequency TEC measurement that adjusts the model estimate for the remaining time in the tracking period.

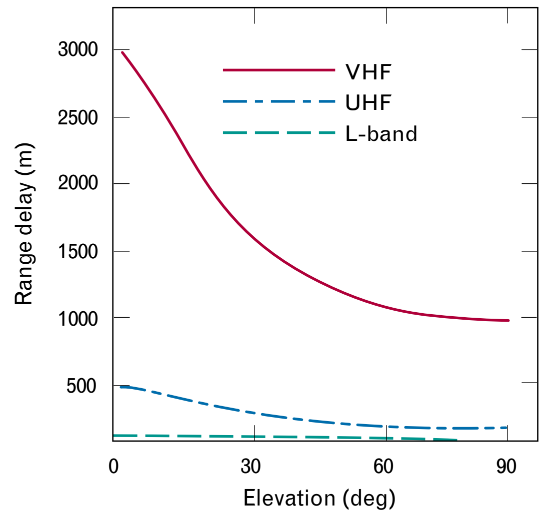

FIGURE 10. Line-of-sight ionospheric range delay determined by using the empirical elevation mapping function. This plot was created for ionospheric conditions with a vertical TEC value of 65.3, or a one-way VHF range delay of 1.0 km. This function maps the vertical line-of-sight TEC or ionospheric range-delay value to an arbitrary elevation. It is derived from historic multifrequency missile data collected at KMR. The figure also illustrates the corresponding ionospheric range delay at UHF and L-band.

ALTAIR First-Order Single-Frequency Ionospheric Range-Delay Model

In the early 1980s, as the number of orbiting satellites increased, ALTAIR single-frequency tracking requirements expanded dramatically for space surveillance. At this time, a first-order vertical ionospheric range-delay model was created to support the continuous single-frequency satellite-tracking and data-collection operations [12]. The first-order model was implemented as a function of time, azimuth, and elevation. The magnitude of the ionospheric range delay (or, similarly, the value of the TEC) at ALTAIR's vertical is determined by the time-dependent component of the first-order model. TEC is proportional to the ionospheric range delay at a particular radio frequency. The model is scaled each day by making a single ALTAIR vertical TEC measurement and then using this measurement to compute the ratio of the range delay (or TEC) measurement to the model value at the measurement time. This ratio is then used to scale the vertical component of the first-order model estimates for the duration of the tracking session, as illustrated in Figure 9.

The second component of the ALTAIR first-order model is the radar elevation mapping function used to extrapolate the vertical TEC value to an arbitrary elevation angle. Figure 10 shows the determination of TEC at VHF, UHF, and L-band, as a function of elevation angle, and Figure 11 shows the determination of elevation-angle bias. During periods of low solar activity this model provides satisfactory results. During periods of moderate to high solar activity the model generally fails to represent actual ionospheric conditions, resulting in degraded range and elevation-angle measurement accuracy by the radar system.

IECM

In 1989, near the peak of the last solar maximum, it became clear that the first-order model failed to meet the ALTAIR satellite-tracking accuracy requirements. The effects of increased solar activity were revealed by the examination of calibration data from the ALTAIR system. ALTAIR measurements (azimuth, elevation,

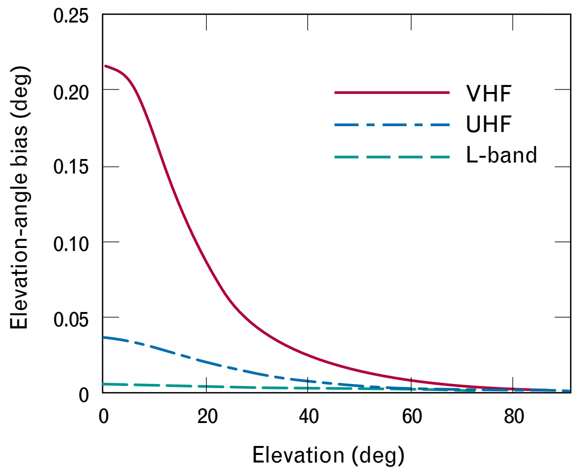

FIGURE 11. Ionospheric elevation-angle bias computed by using the empirical elevation mapping function at VHF, UHF, and L-band. This function is used to estimate the ionospheric elevation-angle bias, given a particular vertical ionospheric range-delay value. This plot was created for ionospheric conditions with a vertical TEC value of 65.3, or a one-way VHF range delay of 1.0 km.

range, and range rate) are compared to precision satellite orbits on a daily basis to monitor and later adjust the calibration parameters of the ALTAIR radar. A modeling shortfall was evident, and this led to the development of the IECM.

Figure 12 illustrates the major components of the IECM. The system was integrated at ALTAIR in 1998 and couples the use of a climatological ionospheric model with real-time ionospheric data from GPS and radar TEC measurements. The IECM consists of four major components: (1) the ionospheric correction algorithm, which provides range and elevation-angle corrections to the radar tracking software from the look-up tables provided by the parameterized electron content model (the ionospheric correction algorithm is the interface to the radar tracking software for atmospheric correction); (2) the parameterized electron content model (PECM), which produces the radar look-up tables (tables of true range and elevation as a function of apparent range, apparent elevation, and azimuth and radar operating frequency); (3) the ionospheric specification manager that is used to manage the communication of the look-up tables to the ionospheric correction algorithm and radar tracking software; and (4) the GPS and radar TEC data-reduction algorithms used to reduce and provide the real-time ionospheric data to the PECM.

The PECM was derived from a global theoretical ionospheric model developed for the U.S. Air Force. This global model, called the parameterized real-time ionospheric specification model (PRISM) was developed by Anderson and R.E. Daniell et al. [18, 19]. The PECM consists of a site-specific, theoretical climatological model (derived from PRISM) that provides a database of the electron content as a function of radar range, elevation angle, and azimuth, and a data-driven update algorithm. The update algorithm adjusts the database of electron content values to match actual conditions. The output of the PECM consists of look-up tables in radar coordinates.

A TEC database specified for application at low latitude is used at ALTAIR. The database used by the PECM is a function of azimuth, elevation angle, and range, relative to the ALTAIR radar site for a specific universal time. Each database electron content table also contains the peak electron-density magnitude and the range to the peak as a function of azimuth and elevation angle. There are 540 database electron content tables covering three seasons (June solstice, December solstice, and equinox), three solar activity levels (high, moderate, and low), and sixty universal times (every thirty minutes for most of the day and every fifteen minutes near dusk and dawn). Each time the PECM runs it reads the date, time, and solar activity index (10-cm solar flux index, $F_{10.7}$). These values are then used to select the particular electron content table from the database. Then the PECM reads the available GPS and radar TEC measurements and adjusts the selected electron content table to match the measured TEC values.

Once the particular database table is updated, a look-up table is produced for the radar by first computing the index of refraction as a function of altitude from the KMR mean tropospheric tables for the neutral atmosphere and updated TEC table for the ionized atmosphere, as shown in Figure 7 [14]. Next, a two-dimensional ray trace is executed to produce two look-up tables (one for each operating frequency at ALTAIR) in radar coordinates. These look-up tables are provided to the radar tracking software and are

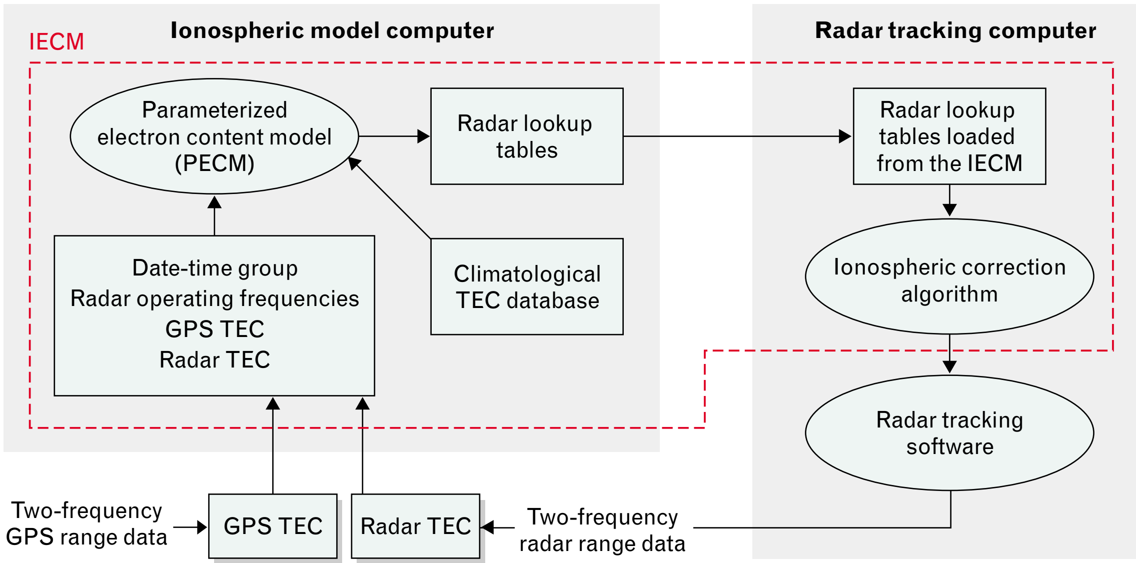

FIGURE 12. Illustration of the major components of the IECM. These components include the climatological TEC database that provides a representative ionosphere, the real-time TEC measurement data that are used to adjust the TEC database to match actual ionospheric conditions, and the parameterized electron content model (PECM) that contains the update algorithms and the ionospheric error-correction algorithm. These PECM algorithms are used to compute the radar look-up tables, which are then provided to the ionospheric correction algorithm in the radar tracking software.

used in conjunction with the ionospheric correction algorithm. The PECM is run at two-minute intervals to take advantage of the high-quality real-time TEC data used to measure actual ionospheric conditions.

Ionospheric Range Delay and TEC

The TEC measurement data described below are provided to the PECM, which consists of update algorithms that use the data to adjust its TEC database to match real-time atmospheric conditions. The method used to deduce line-of-sight ionospheric range delay (or equivalently, time delay) by using two-frequency measurements (also expressed in units of range or TEC) is applied in both the GPS and ALTAIR systems. For GPS, the goal is to remove the atmospheric refraction effects from GPS range measurements to better determine the position and velocity solution for terrestrial navigation purposes [20]. For ALTAIR the goal is to determine the position and velocity of a satellite, minus the distorting effects of the atmosphere. Ideally, all satellites should be tracked by ALTAIR at two frequencies to attain the highest attainable range accuracy. At present, ALTAIR does not have the capability to track satellites at two frequencies beyond near-earth altitude (about five thousand kilometers). Therefore, the aforementioned atmospheric models are applied to correct all data collected with single-frequency radar measurements. This section describes the use of two-frequency range measurements to determine line-of-sight TEC and ionospheric range-delay values for both GPS and the two-frequency ALTAIR system.

Because the group delay in the ionosphere is smaller than the speed of light, a time delay between two points S_1 and S_2 is introduced by the ionosphere at radio frequencies. This delay (in mks units) can be approximated by

$$\delta T = \frac{e^2}{8\pi c m_e \varepsilon f^2} \int_{S_1}^{S_2} N_e \, dS = \frac{40.3}{cf^2} \int_{S_1}^{S_2} N_e \, dS \,, \qquad (2)$$

where c is the speed of light, m_e is the electron mass, e is the electron charge, f is the transmitted frequency, N_e is the electron density, ε is the permittivity constant, and S is the path length of the propagated signal. In the ionosphere, phase delay is advanced by this same amount. The ionospheric range delay (phase advance) in meters is defined as

$$\delta R = c\delta T \, , \tag{3}$$

where this δR is the amount that would be added to the range if the range were calculated by assuming the radar signal traveled at the speed of light. In the case of a target with radar slant range of R, the TEC along the propagation path of the transmitted signal, in units of 10^{16} electrons/m^2, is

$$\text{TEC} = \int_0^R N_e(S)\, dS \, , \tag{4}$$

where $S_1 = 0$ and $S_2 = R$. The integrated electron density N_e (or TEC) is the total number of electrons in a column with height equal to the radar slant range R and a cross-sectional area of one square meter [2, 4, 21].

When a measurement is made at a second frequency, a second equation results, which allows us to solve for TEC:

$$\text{TEC} = \frac{R_2 - R_1}{40.3}\left(\frac{f_1^2 f_2^2}{f_1^2 - f_2^2}\right). \tag{5}$$

The ionospheric range delay δR_1 (in meters) at one of the frequencies is related to the differential range delay $\Delta R = R_2 - R_1$ by

$$\delta R_1 = \Delta R\left(\frac{f_2^2}{f_1^2 - f_2^2}\right). \tag{6}$$

In these equations f_1 and f_2 are the two measurement frequencies, and R_1 and R_2 are the radar slant ranges measured at each frequency. The dispersive property of the ionosphere that causes these signals to refract in a frequency-dependent manner is used to compute the difference between the total time delay (group delay) of the two signals. The total time delay δT is proportional to TEC in units of 10^{16} electrons per unit area (there are no other significant atmospheric sources of microwave frequency-dependent time delay). Once TEC has been calculated, as shown in Equation 5, it is used to estimate the range and elevation-angle corrections needed to determine the true values of a single-frequency radar measurement made in the same vicinity.

The frequency-dependent range delay δR due to the ionosphere and the corresponding TEC correction for ALTAIR's VHF and UHF operating frequencies follow from Equations 5 and 6 as

$$\begin{aligned} \delta R_{\text{VHF}} &= 1.170\,\Delta R\,, \\ \delta R_{\text{UHF}} &= 0.173\,\Delta R\,, \\ \text{TEC} &= 0.0764\,\Delta R\,, \end{aligned}$$

where $\Delta R = R_{\text{VHF}} - R_{\text{UHF}}$ in meters.

Table 3 presents the one-way time delay and corresponding range delay for one TEC unit at VHF and UHF. At low elevation angles, the TEC value can be as large as 333×10^{16} electrons/m^2, which corresponds to range delays of 5100 m (VHF) and 680 m (UHF).

GPS Ionospheric Range Delay

GPS satellites transmit at two L-band frequencies (L1 = 1575.42 MHz and L2 = 1227.6 MHz). The GPS receiver measures the total time delay at L1 and L2. Equations 2 through 6 can be used to express the differential time delay in seconds as

$$T_{\text{L1}} - T_{\text{L2}} = \Delta T_{\text{L}} = \frac{40.3}{c}\,\text{TEC}\left(\frac{f_{\text{L2}}^2 - f_{\text{L1}}^2}{f_{\text{L1}}^2 f_{\text{L2}}^2}\right). \tag{7}$$

For a differential time delay δT_L equal to one nanosecond, the TEC correction is equal to 2.856×10^{16} electrons/m^2. Therefore, there are 2.856 TEC units per nanosecond of differential time delay at the GPS satellite operating frequencies. The integrated electron density for GPS frequencies is expressed, in units of 10^{16} electrons/m^2, as

$$\text{TEC} = 2.856 \times \Delta T_{\text{L}} \, . \tag{8}$$

The measured GPS carrier phase data (at L1 and L2) are used to deduce a more precise value of TEC in real time. At the start of the satellite track, a weighted average of the group and phase TEC are computed. After several minutes of averaging, the difference between the average group TEC and the average phase TEC (ΔTEC) is initialized. This difference is then added to the subsequent phase TEC measurements for the rest of the tracking period, and the result is output to the IECM in real time. The phase TEC

Table 3. Time Delay and Range Delay for One TEC Unit

	VHF (160 MHz)	*UHF (422 MHz)*
δT	51.1 nsec	7.45 nsec
δR	15.35 m	2.26 m

provides a more precise measurement of the rate of change of TEC, but it is biased by an ambiguous number of carrier frequency wavelengths. The difference value ΔTEC removes this bias. Once track has been established on a particular satellite, the differential carrier phase reference is set to zero. If loss of lock (track) is subsequently experienced, the differential carrier phase reference is reinitialized, along with the averaging of group and phase TEC described earlier. Figure 13 illustrates representative GPS TEC data collected at KMR. Each GPS satellite has an associated bias expressed in TEC units. The biases used here were provided by the Jet Propulsion Laboratory [5]. The GPS receiver also has a bias that was estimated by comparing the GPS TEC data to the ALTAIR TEC data.

GPS Receiver Installation and Data Quality

Many experiments were conducted during the period from 1989 to 1997 to learn how to obtain TEC data with sufficient accuracy to support real-time ionospheric correction. This work was performed at the Millstone Hill radar in Westford, Massachusetts, and at the Kwajalein Missile Range, using several GPS receiver models. The first ever real-time ionospheric model based on GPS data was built by Lincoln Laboratory in 1991 [23]. Over the years, several different

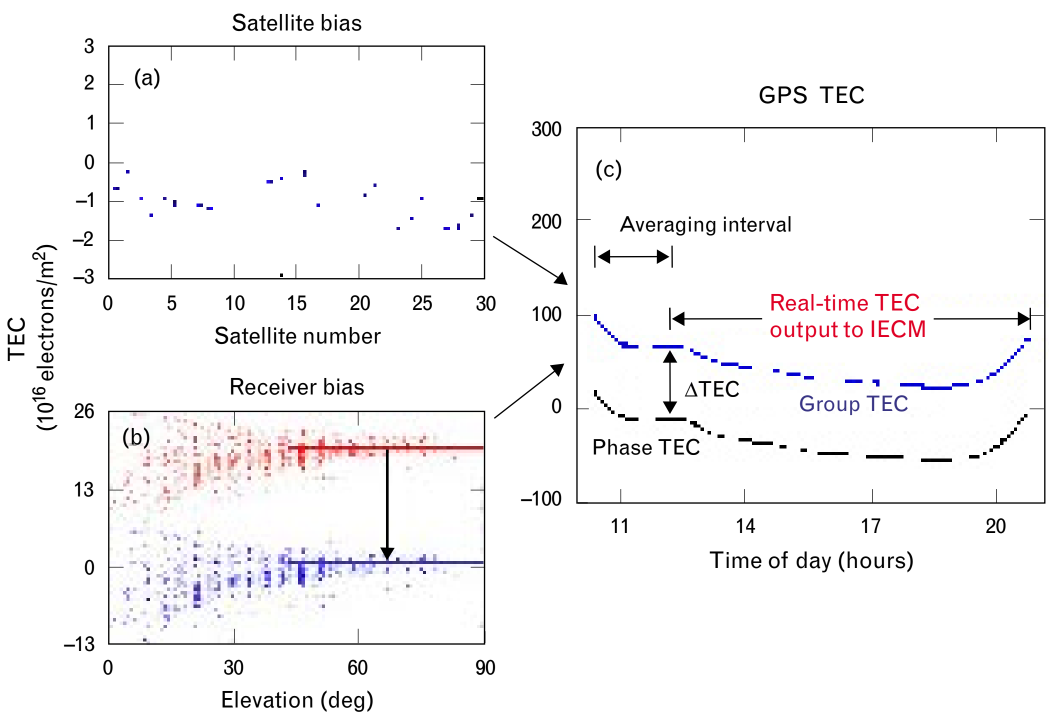

FIGURE 13. Accurate real-time ionospheric measurement data are critical to the performance of the ionospheric models at Kwajalein. This figure shows the real-time reduction of GPS two-frequency data, as illustrated earlier in Figure 8. (a) GPS satellite differential-delay biases in TEC units, computed at the Jet Propulsion Laboratory [22]. (b) Differential-delay bias offset introduced by the GPS receiver, computed by using simultaneous two-frequency tracking data collected at ALTAIR. These values change slowly over time, relative to changes in the ionosphere, and are added to (c) the GPS estimate of the total TEC. The ionosphere affects both the group velocity and phase velocity of the transmitted signals. The estimate of the line-of-sight TEC correction is attained by combining the phase and group measurements collected by the GPS receiver.

GPS receivers and antennas were tested at the two facilities as the technology continued to evolve. The type of antenna and placement of the antenna are important to the reduction of multipath, a critical issue for obtaining accurate real-time TEC data for use at low elevation angles.

The type of GPS receivers evaluated used three different signal processing schemes, which are referred to as precise code, semi-coded, and codeless tracking. While these processing schemes are not described here, it suffices to note that codeless tracking provides the poorest signal-to-noise ratio, while the precise-code signal processing scheme supplies the highest signal-to-noise ratio. In the end an Ashtech ZY-12 receiver (precise code) was determined to provide high-quality TEC. Currently, this receiver is used for real-time operations at ALTAIR. This section summarizes some of the issues encountered in determining GPS data quality, and what was learned by resolving these issues.

The semi-coded GPS receiver provides a 13-dB increase in tracking sensitivity over a codeless receiver in the presence of antispoofing (GPS phase-modulation encryption) by using a proprietary signal processing scheme named Z-mode [24]. With knowledge of the signal encryption, the same semi-coded receiver was able to operate with an additional 17 dB in tracking sensitivity. This additional sensitivity resulted in more precise measurements, especially at low elevation.

Before antispoofing was implemented, the L1 and L2 carrier phases were both modulated and transmitted in the clear with a seven-day (long) pseudo-random noise code (precise code). In the antispoofing mode of operation, the precise code is encrypted into what is called Y-code. In order to take advantage of the Y-code and gain back an overall loss of 30 dB in tracking sensitivity, the GPS receiver must be equipped with secure hardware and firmware. ALTAIR's first receiver was developed before antispoofing was initiated; it automatically reverted to a codeless signal processing scheme [25]. The codeless technique used by the original GPS receiver at ALTAIR resulted in a 30-dB loss in tracking sensitivity over precise-code signal processing. Figure 14 contains representative data to show the increase in the quality of the TEC measurements with codeless,

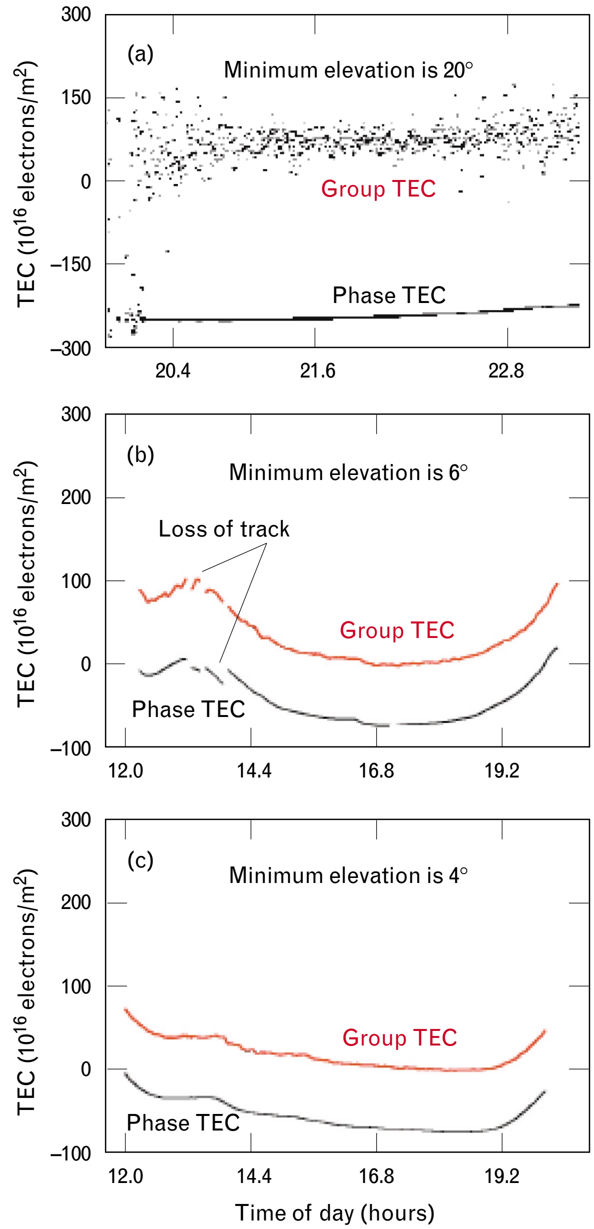

FIGURE 14. TEC data collected at Kwajalein with codeless, semi-codeless, and precise-code tracking. The variability in the TEC data below 20° drove the requirement to use precise-code tracking for the acquisition of accurate TEC measurements. (a) TEC data, collected down to 20°, from the codeless receiver were rendered unusable by the implementation of antispoofing. (b) Semi-codeless tracking down to 6° offers an improvement of 17 dB in tracking sensitivity but still does not provide accurate TEC data at low elevation angle for real-time use below 20°. (c) Precise-code tracking provides a total increase of 30 dB in tracking sensitivity, and high-quality TEC data down to very low elevation angles (4°), compared to codeless tracking. These data are assimilated by the IECM in real time and are essential to obtain accurate real-time TEC corrections for the radar system.

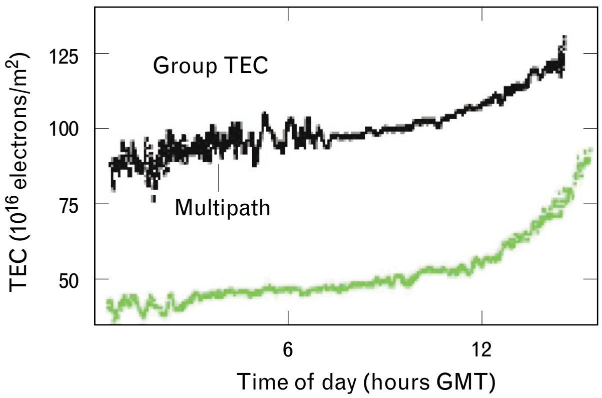

FIGURE 15. GPS TEC data collected near the ALTAIR antenna and at an alternate location where few interference sources were present. These data were collected by using a semi-coded receiver on a GPS satellite, which provided the worse-case multipath data and resulted in a deterministic characterization of multipath sources. The relocation of the GPS antenna to an alternate location eliminated nearly all multipath effects. This GPS receiver was later replaced with a precise-code receiver, further improving the quality of the GPS data by increasing the tracking sensitivity an additional 17 dB.

semi-coded, and precise-code signal processing. The accuracy and precision of these TEC data are critical to obtaining usable real-time ionospheric corrections with the IECM, since these data are assimilated in real time.

The original location for the GPS receiver antenna installation on Roi-Namur was subject to signal multipath from nearby interference sources, as shown in Figure 15. To determine a suitable location for the receiver antenna, TEC data were collected and examined at two other locations on Roi-Namur. The new location for the GPS receiver and antenna was chosen on the basis of a compromise between increased data quality (less multipath) and adequate infrastructure to house the receiver in a temperature-controlled environment and provide communications to send the TEC data to ALTAIR. The new GPS installation was on top of a building, as shown in Figure 16, with the antenna placed at a height above and distant from surrounding obstructions, about three hundred meters from the ALTAIR antenna.

Results

Operational use has shown that the IECM combined with GPS and radar TEC data significantly improves the range-accuracy performance over the first-order ionospheric model while tracking calibration satellites. In great part, this improvement is due to the climatology represented in its TEC database. One of the critical features of the IECM model is that it incorporates the physics of the equatorial region described earlier. In particular, the Appelton anomaly is represented in the model. The first-order ionospheric model originally used at ALTAIR underestimated the azimuthal variation in the TEC distribution. By combining the real-time data from the precise-code GPS receiver, which was installed at ALTAIR in 1998 (and provides up to twelve TEC measurements every ten seconds), and the more complex ionospheric model (the IECM), ALTAIR has a far more accurate representation of the local ionosphere. A precise-code GPS receiver, which has been used to obtain TEC measurements at ALTAIR since 1998, provides a set of up to twelve TEC measurements every ten seconds.

Figure 17 illustrates ALTAIR measurement residuals, on precision reference orbits, collected during 1998 while using both the IECM model and the older first-order ALTAIR model. These data illustrate a significant improvement in the mean range error,

FIGURE 16. A GPS receiver antenna installed near the Kwajalein Atoll lagoon. The ALTAIR antenna shown in the background is approximately three hundred meters from the GPS antenna. The position of this GPS antenna installation, which is well away from and above potential scatterers, eliminated multipath effects from corrupting the TEC correction data at low elevation angles. The yellow boom on the right side of the photo is part of the crane used to lift the photographer to obtain this photograph, and is not a permanent structure that could act as an interference source.

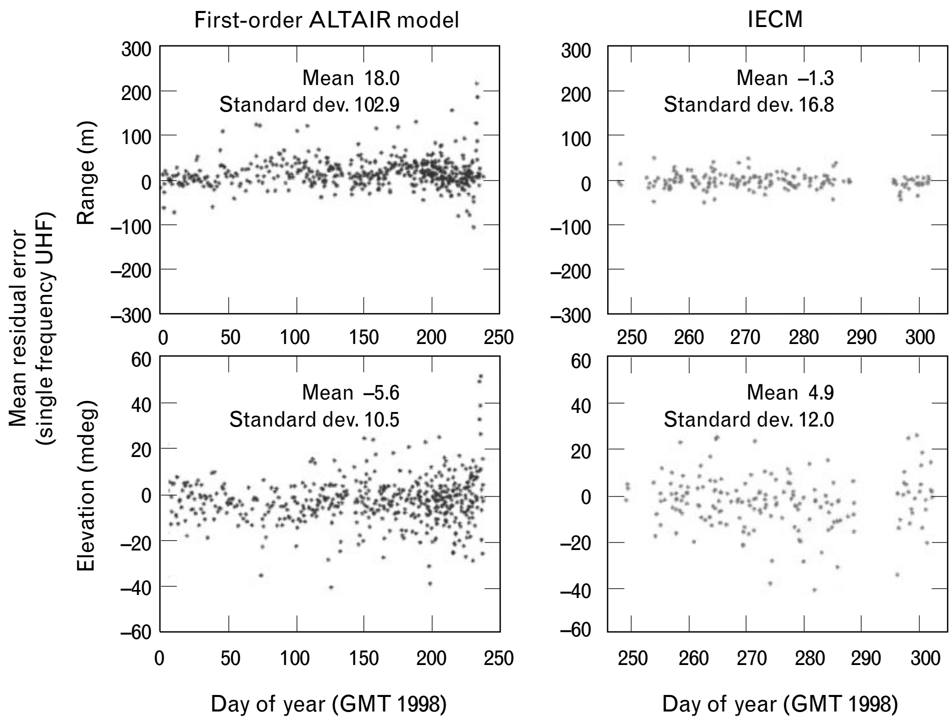

FIGURE 17. Comparison of metric accuracy with the older first-order ALTAIR model and the IECM during 1998. These residual data, which were collected on calibration satellites, result from weekly numerical orbit solutions created with highly accurate laser-ranging data collected by NASA. The tracking data acquired by using the first-order ALTAIR model span approximately 250 days, while the tracking data acquired by using the IECM span nearly sixty days. ALTAIR attained a significant improvement in range accuracy with the IECM, although similar improvements were not apparent in elevation-angle accuracy.

while an improvement in the elevation-angle measurements was not yet realized. This lack of improvement in elevation-angle measurements is possibly due to model error, since the large elevation-angle errors are correlated with the increase in solar activity. A similar system for mid-latitude ionospheric modeling based on GPS was developed at the Millstone Hill Radar in the early 1990s [23].

Future Work

The Kwajalein atmospheric models have been under development since the 1960s, and further study is required to meet KMR's increasing accuracy requirements and national scientific objectives.

In particular, the KMR neutral atmospheric model supplies a mean estimate for the effects of the atmosphere below ninety kilometers in altitude. While the model is useful for real-time application, significant improvements have been accomplished since the time of its implementation. Newer models for estimating tropospheric refraction were developed in the 1980s and 1990s as a consequence of extended research in very long baseline interferometry, satellite laser ranging systems, GPS, and other space-based electromagnetic ranging techniques. The majority of these new models separate out the neutral atmospheric delay into two components: a hydrostatic ("dry") component, and a non-hydrostatic ("wet") component due to the water vapor in the atmosphere. An excellent review of these models can be found elsewhere [26]. The next logical area of research and application involves the incorporation of one of these models into the IECM, for example, the atmospheric model developed for the FAA's Wide Area Augmentation System [27].

At the time IECM was developed, the capacity of the available computers forced compromises in the size of the climatological TEC database that represented the ionosphere, thereby affecting model resolution. At present, these tables are implemented as a function of season and solar activity; there is a characterization of three seasons and solar activity levels. A better characterization of the representative ionosphere would result from the creation and use of TEC models for each month and solar activity period. This expansion would vastly increase the number of tables and increase the granularity of the representative ionosphere by merely taking advantage of the greater capabilities in present computer technology.

The IECM alone does not provide an accurate representation of the actual ionospheric conditions, but when the IECM is combined with real-time GPS TEC measurements, it provides a significant improvement over the first-order ALTAIR model. While GPS TEC measurements are significant, on their own they provide little or no real-time information on the ionospheric distribution and structure, which is especially important in the equatorial region. To obtain information on the ionospheric profile, measurements such as those obtained from a digital high-frequency ionospheric sounder (ionosonde) or incoherent scatter are needed. Another approach would involve the implementation of tomography receivers and software to reconstruct the ionosphere through tomographic imaging techniques combined with TEC measurements [28]. The best approach would be to combine many different systems of measurement collection and then provide the data to IECM.

Summary

Background on the equatorial ionosphere has been summarized to provide support for the emphasis of current research and model application. The properties of the equatorial ionosphere drive the need for a representative model to accompany real-time measurement data when attempts are made to model the state of the ionosphere at any given time. This need for a model is due to a limited amount of measurement data relative to the complex structure of the equatorial ionosphere. To rectify this shortfall, the IECM—a climatological model that provides a representative ionosphere—has been in operational use at KMR since 1998.

The collection of real-time ionospheric measurements to adjust the IECM to match actual conditions has proven to be the best technique to resolve model accuracy issues. The improvement in radar range accuracy brought about by the use of IECM combined with real-time GPS TEC is clearly illustrated. Further improvement in accuracy would be realized if additional real-time ionospheric measurement data (such as that provided from an on-site ionosonde) could be provided to the IECM. Proving the accuracy of the ionospheric models relative to a fundamental truth is a strength that the KMR radar systems bring to bear on the problem. Their precise calibration and access to "ground truth" using accurate calibration satellite orbits is the basis for the error analysis presented here.

Acknowledgments

Art Lewis of Raytheon has contributed to the design, development, and integration of the KMR models for over twenty years. Mike Austin of the Field Systems group at Lincoln Laboratory submitted the request for and managed the Small Business Innovative Research contract that led to the IECM. Greg Hogan of the Field Systems group contributed to the contents of this document. George Millman and Jeff Lamicela of Research Associates of Syracuse, Inc., Syracuse, New York, and Rob Daniell and Lincoln Brown of Computational Physics, Inc., in Newton, Massachusetts, developed the IECM for its application at ALTAIR under the Small Business Innovative Research contract. Lorraine Thornton of the Surveillance Techniques group at Lincoln Laboratory provided the precise calibration data used to evaluate the accuracy of the IECM. Dale Sponseller from Raytheon at Kwajalein provided technical support in the integration of the GPS receiver equipment at ALTAIR. Anthony Manucci, Brian Wilson, and Garth Franklin of the Jet Propulsion Laboratory provided guidance in the installation of the GPS receiver equipment and supplied the GPS satellite calibration biases applied in the IECM.

REFERENCES

1. MIT Haystack Observatory Web Site, <http://www.haystack.edu/ysp/atmosphere/earth.html>, June 1, 1999.
2. J.W. Chamberlain and D.M. Hunten, *Theory of Planetary Atmospheres: An Introduction to Their Physics and Chemistry (*Academic Press, Orlando, Fla., 1987).
3. T.I. Gambosi, *Physics of the Space Environment,* Cambridge Atmospheric and Space Science Series (Cambridge University Press, Cambridge, U.K., 1998), pp. 177–189.
4. A. Jursa, ed., *Handbook of Geophysics and the Space Environment* (Air Force Geophysics Laboratory, Air Force Systems Command, U.S. Air Force, 1985).
5. M.C. Kelley, *The Earth's Ionosphere: Plasma Physics and Electrodynamics* (Academic Press, San Diego, 1989).
6. R.J. Moffet, "The Equatorial Anomaly in the Electron Distribution of the Terrestrial F-Region," *Fundam. Cosmic Phys.* **4,** 1979, pp. 313–391.
7. M. Mendillo, J. Baumgardner, X. Pi, P.J. Sultan and R. Tsunoda, "Onset Conditions for Equatorial Spread F," *J. Geophys. Res.* **97** (A9), 1992, pp. 13,865–13,876.
8. R.T. Tsunoda, "Time Evolution and Dynamics of Equatorial Backscatter Plumes. 1. Growth Phase," *J. Geophys. Res.* **86** (A1), 1981, pp. 139–149.
9. R.T. Tsunoda, "Magnetic-Field-Aligned Characteristics of Plasma Bubbles in the Nighttime Equatorial Ionosphere," *J. Atmos. Terr. Phys.* **42** (8), 1980, pp. 743–752.
10. J.K. Hargreaves, *The Solar-Terrestrial Environment: An Introduction to Geospace,* Cambridge Atmospheric and Space Science Series (Cambridge University Press, Cambridge, U.K., 1992).
11. W.E. Swartz and R.F. Woodman, "Same Night Observations of Spread-F by the Jicamarca Radio Observatory in Peru and CUPRI in Alcantara, Brazil," *Geophys. Res. Lett.* **25** (1), 1998, pp. 17–20.
12. R. McSheehy, private communication, Group 33, Lincoln Laboratory, 1992.
13. J. Klobuchar and R. Allen, "A First Order, Worldwide, Ionospheric Time Delay Algorithm," AFCRL-TR-75-0502, AFCRL(LI), Hanscom AFB (25 Sept 1975), DTIC #AD-A018862.
14. R.E. Daniell, Jr., L.D. Brown, D.N. Anderson, M.W. Fox, P.H. Doherty, D.T. Decker, J.J. Sojka, and R.W. Schunk, "Parametrical Ionospheric Model: A Global Parameterization Based on First Principles Models," *Radio Sci.* **30** (5), 1995, pp. 1499–1510.
15. G. Millman, Research Associates of Syracuse, Inc., Syracuse, New York, private communication, June 1998.
16. D.N. Anderson, M. Mendillo, and B. Herniter, "A Semi-Empirical Low-Latitude Ionospheric Model," *Radio Sci.* **22** (2), 1987, pp. 292–306.
17. D.L. Gallagher, P.D. Craven, and R.H. Comfort, "An Empirical Model of the Earth's Plasmasphere," *Adv. Space Res.* **8,** 1988, pp. (8)15–(8)24.
18. D.N. Anderson, "The Development of Global, Semi-Empirical Ionospheric Specification Models," *Proc. Ionospheric Effects Symp., Alexandria, Va., 4–6 May 1993,* pp. 4B/3/1–3.
19. R.E. Daniell, Jr., W.G. Whartenby, and D.N. Anderson, "PRISM Validation," *Proc. Ionospheric Effects Symp., Alexandria, Va., 4–6 May 1993,* pp. 4B/2/1–11.
20. J.J. Spilker, Jr., "GPS Signal Structure and Performance Characteristics," *Navig. J. Inst. Navig.* **25** (2), 1978, pp. 121–146.
21. D. Coco, "GPS—Satellites of Opportunity for Ionospheric Modeling," *GPS World* **2** (10), 1991, pp. 47–50.
22. A. Mannuci and B. Wilson, Jet Propulsion Laboratory, private communication, June 1997.
23. A.J. Coster, E.M. Gaposchkin, and L.E. Thornton, "Real-Time Ionospheric Monitoring System Using GPS," *Navig. J. Inst. Navig.* **39** (2), 1992, pp. 191–204.
24. *Ashtech Z-12 GPS Operating Manual,* Ashtech Document Number 600224, May 1994.
25. *Technical Manual for the Model ICS-4Z Mini-Rogue,* Allen Osborne Assoc., June 1992.
26. V. de Brito Mendes, "Modeling the Neutral-Atmospheric Delay in Radiometric Space Techniques," Technical Report No. 199, University of New Brunswick, Geodesy and Geomatics Engineering, Apr. 1999.
27. P. Collins and R.B. Langley, "Tropospheric Delay—Prediction for the WAAS User," *GPS World* **10** (7), 1999, pp. 52–58.
28. G. Bust, T.L. Gaussiran II, and D.S. Coco, "Ionospheric Observations of the November 1993 Storm," *J. Geophys. Res.* **102** (A7), 1997, pp. 14,293–14,304.

STEPHEN M. HUNT
is an associate staff member in the Field Systems group. He is the system analyst of the Kwajalein Space Surveillance Center, which is used to conduct the remote operation and measurement-data reduction for the radar systems at Kwajalein. He received a B.S. degree in physics from Worcester Polytechnic Institute and is currently pursuing a graduate degree in space physics at Boston University. Prior to his current position he worked in the Space Surveillance Techniques group, including several years at the Kwajalein Missile Range. At Kwajalein he was a space-surveillance analyst, and he participated in a collaborative effort to characterize meteors by using the ARPA Long Range Tracking and Instrumentation Radar (ALTAIR). He was also responsible for the development and integration of a real-time ionospheric modeling system for ALTAIR.

SIGRID CLOSE
is an associate staff member at the Kwajalein Missile Range field site, where her primary duty is in space surveillance at ALTAIR, including orbital analysis for operational space-launch tracking support, routine spacecraft monitoring, and unplanned space-surveillance events. Her interests also include ionospheric modeling and analysis, as well as meteor research. Previously she worked for the Advanced Electromagnetic Systems group at Lincoln Laboratory in the area of radar phenomenology. She has a B.S. degree in physics and astronomy from the University of Rochester, and an M.S. degree in physics from the University of Texas at Austin, where her graduate thesis involved the study of gravity waves in plasmas.

ANTHEA J. COSTER
is a staff member in the Surveillance Techniques group. She received a B.A. degree in mathematics from the University of Texas at Austin, and M.S. and Ph.D. degrees in space physics and astronomy from Rice University, where she was involved with ionospheric heating experiments at the Arecibo Observatory in Puerto Rico. At Lincoln Laboratory she has been responsible for the development of software and hardware used to compensate for atmospheric refraction at the Millstone Hill radar. Together with her coworkers, she developed the first real-time ionospheric monitoring system based on GPS. This system is now an integral part of the MIT radar calibration system. In 1995, she was awarded an Advanced Concepts Program grant to conduct the Westford Water Vapor experiment, which verified that GPS could be used to obtain accurate, near-real-time information on the amount of water vapor present in the atmosphere. She is a member of the International Union of Radio Science (URSI), the Institute of Navigation (ION), and the American Geophysical Union. She is the current vice-chair of commission G (ionosphere), U.S. chapter of URSI, a member of the GPS Meteorology Interagency Working Group, and a recent technical chair for the September 2000 ION-GPS meeting.

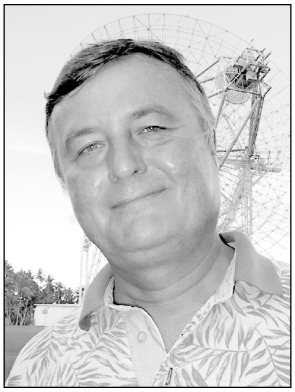

ERIC STEVENS
is an orbital analyst in the Field Systems group at Kwajalein Missile Range. He attended the University of New Hampshire, where he majored in mechanical engineering before switching to computer science. His work at Kwajalein has focused on adding new capabilities to the ALTAIR deep-space tracking system, including ionospheric correction. Prior to coming to ALTAIR he was leader of the software section of the Aerospace Engineering group. He recently retired after thirty-two years at Lincoln Laboratory.

LINDA M. SCHUETT
is a systems engineer for Raytheon Range Systems Engineering at Kwajalein Missile Range. Her primary duty is systems support at the ALTAIR radar, including mission planning and directorship, radar upgrade analysis and testing, and engineering support for the radar ionospheric correction model. Her primary research interests include radar signal processing, space surveillance, and radar ionospheric correction. Previously she was at the Georgia Tech Research Institute (GTRI), working in areas of electronic warfare modeling and analysis, and teaching sessions of a radar course. Previous to GTRI she was at the Westinghouse Defense Center, working in electronic warfare, advanced systems development, and system test support. She received a B.S. in electrical engineering from Valparaiso University, and an M.S. in electrical engineering from the Georgia Institute of Technology.

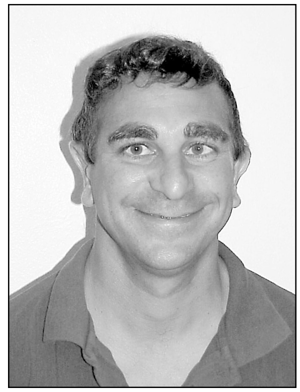

ANTHONY VARDARO
is a software engineer with Raytheon Corporation at the Kwajalein Missile Range. Previously he was a Lincoln Laboratory contractor for nine years, working with the Laser Radar group and the Air Traffic Automation group. He received B.S.E.E. and M.S.E.E. degrees from Northeastern University.